

Article

Alkali-Free Hydrothermally Reconstructed NiAl Layered Double Hydroxides for Catalytic Transesterification

Nazrizawati A. Tajuddin ¹, Jinesh C. Manayil ², Adam F. Lee ³ and Karen Wilson ^{3,*}

¹ School of Chemistry and Environment, Faculty of Applied Sciences, University of Technology MARA, Shah Alam 40450, Malaysia; nazriza@uitm.edu.my

² Energy & Bioproducts Research Institute (EBRI), Aston University, Birmingham B4 7ET, UK; j.manayil@aston.ac.uk

³ Centre for Applied Materials & Industrial Chemistry (CAMIC), School of Science, RMIT University, 124 La Trobe Street, Melbourne, VIC 3000, Australia; adam.lee2@rmit.edu.au

* Correspondence: karen.wilson2@rmit.edu.au

Abstract: NiAl layered double hydroxides (LDHs) are promising bifunctional catalysts comprising tunable redox and Lewis acidic sites. However, most studies of NiAl LDH employ alkali hydroxide carbonate precipitants which may contaminate the final LDH catalyst and leach into reaction media. Here, we report an alkali-free route to prepare Ni_xAl LDHs with a composition range $x = 1.7$ to 4.1 using (NH₄)₂CO₃ and NH₄OH as precipitants. Activation of LDHs by calcination–rehydration protocols reveal Ni_xAl LDHs can be reconstructed under mild hydrothermal treatment (110 °C for 12 h), with the degree of reconstruction increasing with Ni content. Catalyst activity for tributyrin transesterification with methanol was found to increase with Ni content and corresponding base site loadings; TOFs also increased, suggesting that base sites in the reconstructed LDH are more effective for transesterification. Hydrothermally reconstructed Ni_{4.1}Al LDH was active for the transesterification of C₄–C₁₂ triglycerides with methanol and was stable towards leaching during transesterification.

Keywords: biodiesel; layered double hydroxides; transesterification; hydrothermal; nickel; aluminum; solid base



Citation: Tajuddin, N.A.; Manayil, J.C.; Lee, A.F.; Wilson, K. Alkali-Free Hydrothermally Reconstructed NiAl Layered Double Hydroxides for Catalytic Transesterification. *Catalysts* **2022**, *12*, 286. <https://doi.org/10.3390/catal12030286>

Academic Editors: Ioan-Cezar Marcu and Octavian Dumitru Pavel

Received: 11 January 2022

Accepted: 20 February 2022

Published: 3 March 2022

Publisher's Note: MDPI stays neutral with regard to jurisdictional claims in published maps and institutional affiliations.



Copyright: © 2022 by the authors. Licensee MDPI, Basel, Switzerland. This article is an open access article distributed under the terms and conditions of the Creative Commons Attribution (CC BY) license (<https://creativecommons.org/licenses/by/4.0/>).

1. Introduction

Layered double hydroxides (LDH) of general formula $[M^{2+}_{(1-x)}Al^{3+}_x(OH)_2]^{x+}(A^{n-})_{x/n} \cdot yH_2O$ are interesting materials for photo-, electro-, and thermocatalysis [1,2] and electronic applications [3–5]. They typically adopt three-dimensional, lamellar structures of mixed metal oxyhydroxide platelets, with the interlayer voids providing nanoporous chemical reactors [6]. The catalytic versatility of LDHs arises from their structural flexibility, wherein a range of divalent M^{2+} and trivalent M^{3+} cations can be introduced into the platelets and diverse charge-balancing anions A^{n-} (e.g., CO_3^{2-} , SO_4^{2-} , Cl^- , OH^-) within the interlayers [7,8]. Consequently, LDHs offer tunable redox and electronic properties and morphologies amenable to delamination into individual two-dimensional platelets [9] or assembly into complex architectures such as sand roses [10,11]. The morphology of LDHs is largely dictated by their synthesis; low temperature co-precipitation favors random lamellar arrangements in which precursor impurities are retained [9], whereas moderate temperature calcination to remove impurities necessitates subsequent reconstruction [12,13] of mixed metal oxide crystallites by hydrothermal treatment to recover lamellar structures (calcination–rehydration) [14–18].

LDHs featuring transition metals such as Co, Fe, or Ni as divalent cations have been the focus of electrocatalytic applications [19] due to their good conductivity [20], low cost, and ease of generating host structures with high proton mobility [19]. NiAl LDH materials also find widespread application as precursors to Ni/Al₂O₃ catalysts [21] for

hydrogenation/hydrodeoxygenation [19,22], H₂ production by steam reforming [23], and lignin depolymerization/hydrogenolysis [24].

LDH materials are typically synthesized by the coprecipitation of soluble M²⁺/M³⁺ ionic solutions using NaOH or KOH, in the presence of the corresponding counter ion, typically CO₃²⁻ [8,25]. The use of ammonia or urea as a precipitating agent is preferable for applications where intercalated alkali cations from the residual precipitating agent could impair performance of the resulting LDH [26–28]. While routes such as hydrothermal urea hydrolysis [29] have been employed to prepare NiAl LDHs, the use of NH₄CO₃/NH₄OH precipitants has not been explored, to our knowledge, and may offer milder synthesis conditions.

Activation of LDH materials is often required to increase their catalytic utility [16]. This commonly involves calcination to decompose the precipitated LDH by removing charge compensating anions (accompanied by dehydroxylation) to form an amorphous mixed oxide. Reconstruction of these mixed oxides into lamellar structures is observed on subsequent hydration, termed the ‘memory effect’, which also introduces vacancies into the metal oxyhydroxide layers, due to the replacement of interlayer CO₃²⁻ with OH⁻ [30,31]. Calcined MgAl LDH materials can be readily reconstructed by vapor phase rehydration [12,32], but relies on moderate temperature (<550 °C) calcination to avoid significant formation of tetrahedral Al³⁺ and spinel structures [33]. Indeed, not all calcined LDHs can be fully reconstructed by such treatments, as the partial oxidation of the M²⁺ cation or the formation of thermodynamically stable mixed oxides are also possible [34]. A consequence is that calcined ZnAl LDH requires more forcing hydrothermal treatments to partially regenerate the initial lamella structure, due to the stability of Al(OH) and ZnO formed on calcination [28]. NiAl LDH materials are also challenging to reconstruct due to the formation of Al-doped NiO and spinel-like phases at elevated temperatures [21,35,36]. The influence of the Ni:Al ratio on the hydrothermal reconstruction of calcined NiAl LDH prepared by NH₄OH/NH₄CO₃ precipitation has not been previously reported. However, as alkali-free precipitants typically yield smaller LDH crystallites than their alkali analogues [26], these may be more susceptible toward reconstruction.

NiAl LDH materials are expected to exhibit mild basic properties (albeit weaker than for MgAl LDH, due to the lower electropositivity of the transition metal) [36,37], and hence may be suitable for base-catalyzed reactions. Here, we explore the hydrothermal reconstruction and catalytic activity of a family of NiAl LDHs for the transesterification of model (C4-C12) triglycerides to fatty acid methyl esters (FAME).

2. Results and Discussion

2.1. Catalyst Characterisation

The successful synthesis of alkali-free NiAl LDH materials was verified by XRD, SEM, and EDS. XRD reflections of the as-precipitated LDHs (Figure 1a) were in good agreement with reference patterns for the takovite structure (JSPDS 15-0087), while EDS confirmed that Ni:Al bulk atomic ratios were similar (albeit slightly higher) to their nominal values, varying between 1.7:1 and 4.1:1 across the LDH family (Table 1). Corresponding BET surface areas were also in accordance with literature values for NiAl LDHs, spanning 260–60 m²·g⁻¹ [8]. Surface areas of LDH materials are a complex convolution of crystallite size and density; however, for the same morphology, increased Ni content is expected to lead to a decrease in the specific surface area. NiAl LDH compositions were also estimated from TGA by quantifying weight losses attributed to the desorption of intercalated H₂O (~150 °C) and CO₃²⁻ decomposition (261–355 °C) (Table S1 and Figure S2) and are in good agreement with expectations [38,39]. Higher Ni loadings are expected to expand the interlayers, thereby increasing water intercalation.

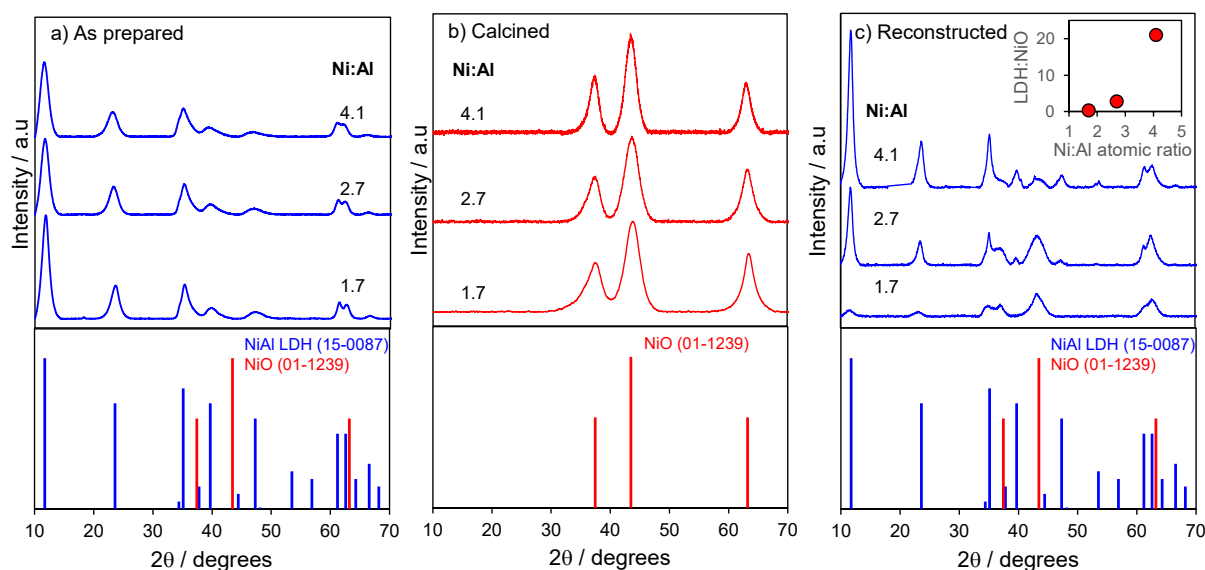


Figure 1. Powder XRD patterns of (a) As-prepared; (b) Calcined; and (c) Hydrothermally reconstructed, alkali-free NiAl LDH materials.

Table 1. Physicochemical properties of as-prepared and reconstructed NiAl LDH materials.

As-Prepared					Reconstructed		
Nominal Ni:Al Atomic Ratio	Bulk Ni:Al Atomic Ratio ^a	Surface Ni:Al Atomic Ratio ^b	NiAl LDH Formula ^c	BET Surface Area ^d /m ² ·g ⁻¹	BET Surface Area ^d /m ² ·g ⁻¹	Base Site Loading ^e /mmol·g ⁻¹	Base Site Loading /Molecules·g ⁻¹
1.5:1	1.7:1	1.0	[Ni _{0.6} Al _{0.4} (OH) ₂].(CO ₃) _{0.18} 0.56H ₂ O	149	183	0.062	3.7 × 10 ¹⁹
3:1	2.7:1	2.6	[Ni _{0.7} Al _{0.3} (OH) ₂].(CO ₃) _{0.14} 0.58H ₂ O	236	207	0.072	4.4 × 10 ¹⁹
4:1	4.1:1	4.1	[Ni _{0.8} Al _{0.2} (OH) ₂].(CO ₃) _{0.10} 0.72H ₂ O	77	134	0.099	6.0 × 10 ¹⁹

^a from EDX (error ±0.13), ^b from XPS, ^c CO₃²⁻, and H₂O quantified by TGA, ^d Standard error ±30 m²·g⁻¹, ^e from CO₂ pulse chemisorption.

A comparison of surface and bulk Ni compositions from XPS and EDS, respectively, confirm an expected linear relationship for a pure phase LDH (Figure S1a) and, hence, a negligible surface segregation of Ni or Al pure phases. Ni 2p XP spectra of the NiAl LDHs (Figure S1b) reveal a well-resolved spin-orbit split doublet with 2p_{3/2} and 2p_{1/2} peaks at 854 eV and 872 eV binding energies, respectively, and shake-up satellites at 860 eV and 879 eV consistent with Ni²⁺ [40]. Corresponding Al 2p XP spectra reveal a similar spin-orbit split doublet with a 2p_{3/2} peak at 75.2 eV consistent with Al³⁺ in an LDH. Activation of NiAl LDHs by calcination and hydrothermal reconstruction was subsequently assessed. A 350 °C calcination temperature was selected as this achieved sufficient dehydroxylation/decarbonylation to destruct the ordered LDH phase in all materials (Figure S2) while also minimizing sintering. All calcined NiAl LDHs exhibited reflections at 37.4°, 43.9°, and 63.3° (Figure 1b), consistent with the formation of NiO (JSPDS 01-1239) [41]. The genesis of a crystalline NiAl₂O₄ spinel phase was not observed, and requires higher temperatures (~900 °C) [42]. Calcination at 350 °C thus generates NiO crystallites and amorphous alumina, similar to previous reports [38,43,44]. Higher temperature calcination of an alkali-precipitated Ni₂Al LDH reports the formation of an Al-containing NiO-like oxide at 450 °C alongside an Al-rich amorphous component. Previous Rietveld refinement also revealed a smaller lattice parameter for the former phase than observed for pure NiO (lattice parameter of 0.418 nm) [43], which increased with Ni:Al content of the parent LDH. A slight increase in the lattice parameter (determined from the d(200) reflection) of the NiO phase with Ni:Al ratio was also observed for our NiAl LDHs (from 0.413 to 0.416 nm); this indicates that trace Al must likewise be incorporated into alkali-free NiO crystallites obtained after 350 °C calcination.

The reconstruction of 350 °C calcined NiAl LDHs was subsequently attempted at 110 °C in water. Note that it was not possible to reconstruct calcined NiAl LDHs using

water vapor (Figure S3) in accordance with previous reports [21,35,36]. The complete reconstruction of calcined LDHs requires rehydration of mixed metal oxides and dissolution of any segregated M^{2+} oxide, which for Ni^{2+} requires more forcing conditions owing to the formation of stable (NiAl)O mixed oxides on calcination [13].

Hydrothermal treatments have proven more effective than water vapor in reconstructing the lamellar structure of calcined MgAl [45] and ZnAl [28] LDHs. In the present work, recovery of an LDH phase was strongly dependent on the Ni:Al ratio in the parent material (Figure 1c), with $Ni_{1.7}Al$ and $Ni_{2.7}Al$ LDHs retaining significant NiO. In contrast, the $Ni_{4.1}Al$ material exhibited negligible NiO and a majority reconstructed LDH phase, with the lattice parameter for the *c* axis determined to be 2.25 nm (calculated from the *d*(006) reflection at 23.6°). This is almost identical to that for the parent material (2.26 nm), and corresponds to an interlayer spacing (*d*) of 0.75 nm (note lattice parameter $c = 3d$ [46]). This observation is significant since it is generally regarded that reconstruction of calcined NiAl LDHs by rehydration alone is not possible and requires harsh conditions (e.g., $160^\circ C$ in NH_4OH) [36]. Successful hydrothermal reconstruction in this work may reflect enhanced Al incorporation into the NiO phase obtained by lower temperature ($350^\circ C$) calcination versus literature reports, and concomitantly less phase-separated tetrahedral Al^{3+} (difficult to reincorporate during LDH reconstruction [33]).

The morphology of the $Ni_{4.1}Al$ LDH was studied by SEM following calcination and hydrothermal reconstruction (Figure 2). The precipitated NiAl LDH exhibited a characteristic sand-rose structure comprising assemblies of fused platelets. These structures evolve due to initially fast crystallisation of LDH seeds which preferentially grow along their (001) planes, disfavoring nanoparticle aggregation [47]. HRTEM (Figure S4) reveals the lattice spacing of LDH crystallites within precipitated platelets as 0.33 nm, corresponding to the *d*(110) plane, which is slightly larger than that determined from the corresponding XRD reflection but within the range expected for LDH lattice fringes. Calcination transforms the parent LDH into spherical agglomerates (Figure 2b), which are converted back to a fused lamellar structure by hydrothermal treatment (Figure 2c). Lattice fringes of the reconstructed $Ni_{4.1}Al$ LDH were determined by XRD and HRTEM as 0.30 and 0.31 nm, respectively. Slight contractions in the interlayer spacing relative to the parent material are attributed to the replacement of interlayer CO_3^{2-} by OH^- anions. NiAl LDHs are expected to exhibit basic character, originating from undercoordinated oxygen sites or Me–OH surface groups formed to charge balanced Al^{3+} ions replaced by Ni^{2+} in LDH layers as the Ni:Al ratio increases [48]. The quantification of base site loadings by CO_2 pulse chemisorption confirmed that basicity increases with Ni:Al ratio (Table 1).

2.2. Transesterification Activity

The impact of Ni:Al ratio on the activity of reconstructed NiAl LDHs was subsequently evaluated for the base-catalyzed transesterification of tributyrin with methanol (Figures 3 and S5).

TOFs increased from 60 to 180 h^{-1} with rising Ni:Al ratio, mirroring the trends in conversion (which ranged from 15% to 30% over 6 h reaction) (see Figure S5), indicative of increased accessibility or base strength of active sites, the former being consistent with a greater extent of hydrothermal reconstruction observed by XRD (Figure 1c inset). These TOFs are in line with literature values for tributyrin transesterification over related ZnAl ($180\text{--}290\text{ h}^{-1}$) [28] and Mg_2Al (329 h^{-1}) [45,49] LDHs, considering their relative basicity ($NiAl \approx ZnAl < MgAl$ [16,50]), which are comparable to values for nanocrystalline MgO (220 h^{-1}) [51] and Mg– ZrO_2 (100 h^{-1}) [52]. Selectivity to methyl butyrate was $>95\text{--}80\%$, with a slight decrease observed with Ni:Al ratio attributed to increased conversion across the series, and reduced transesterification activity of diglycerides (see discussion later) [53].

The most active $Ni_{4.1}Al$ LDH catalyst was selected for the transesterification of longer-chain $C_8\text{--}C_{12}$ TAGs (Figure 4 and Figure S6). $Ni_{4.1}Al$ LDH was active for all three TAGs; however, conversions and TOFs fell with increasing alkyl chain length, likely reflecting poorer base site accessibility for the bulkier TAGs [45]. FAME selectivities also fell with

increasing chain length, reaching ~40% for trilaurin after 24 reaction, suggesting poor mass transport [45,54] of bulky diglyceride (DAG) and monoglyceride (MAG) reactively-formed intermediates, and that their competitive adsorption with TAG hinders subsequent conversion under batch conditions [55,56]. Slow DAG conversion has previously been accounted for, owing to activation barriers for transesterification being higher than for their corresponding triglycerides. The removal of the first fatty acid chain leads to increased electron density at the $-\text{CH}_2\text{-OH}$ center of the glyceride backbone, which hinders subsequent attack by adsorbed MeO^- at the remaining ester groups [53].

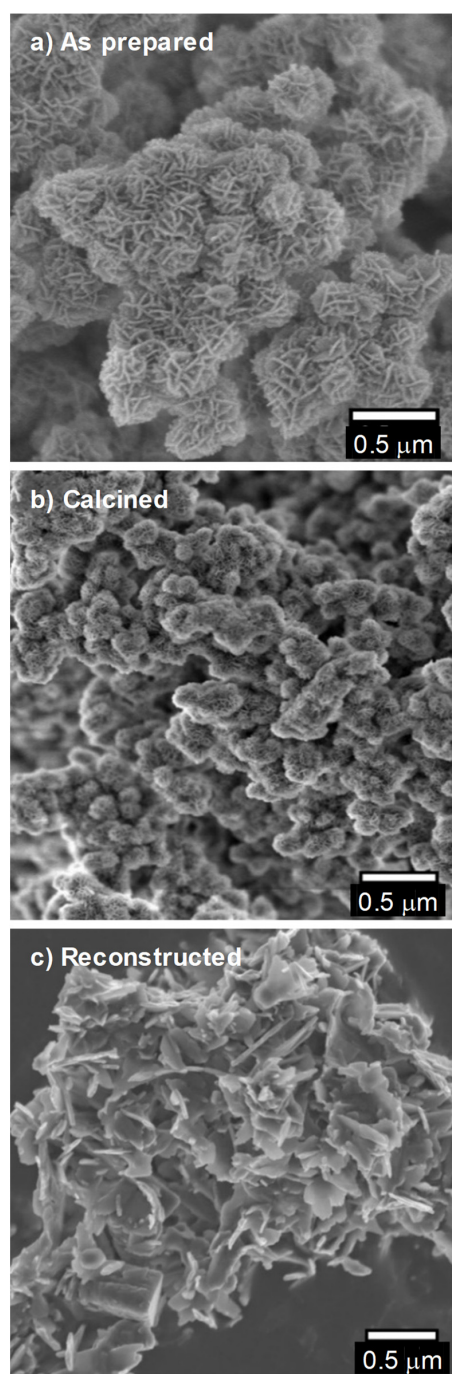


Figure 2. SEM images of (a) As-prepared; (b) Calcined; and (c) Hydrothermally reconstructed, alkali-free Ni_{4.1}Al LDH materials.

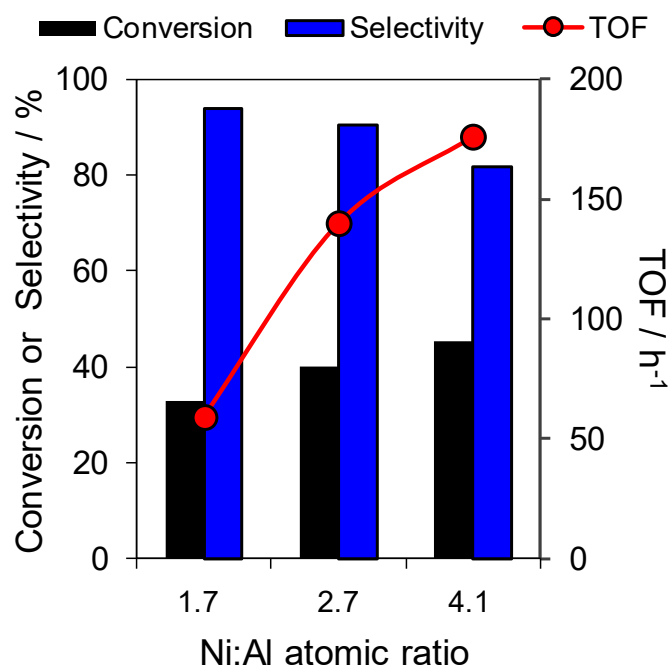


Figure 3. Activity of reconstructed NiAl LDH for transesterification of tributyrin with methanol as a function of Ni:Al ratio; conversion and selectivity after 24 h, TOF from initial rate over 1 h reaction. Reaction conditions: 100 mg catalyst, 110 °C, 10 mmol TAG, 30:1 methanol:TAG molar ratio, 650 rpm stirring.

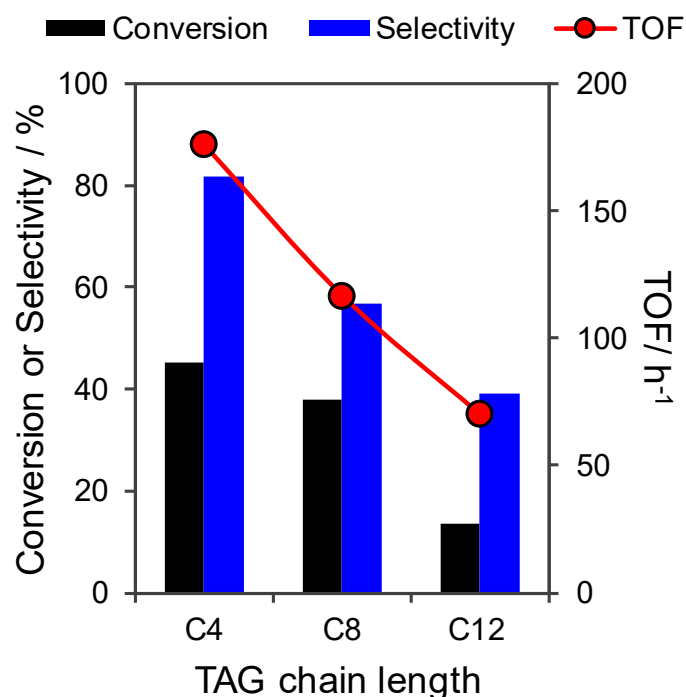


Figure 4. Catalytic performance of reconstructed Ni_{4.1}Al LDH for transesterification of C₄-C₁₂ TAGs with methanol; conversion and selectivity values after 24 h, TOF calculated from initial rate over 1 h reaction. Reaction conditions: 100 mg catalyst, 110 °C, 10 mmol TAG, 30:1 methanol:TAG molar ratio (20 wt% 1-butanol for C₈-C₁₂ TAG), 650 rpm stirring.

The stability of the Ni_{4.1}Al LDH catalyst was investigated by a recycling study for tributyrin transesterification, which confirmed the heterogenous nature of the catalysis (Figure S7). The same catalyst could be recycled, retaining ~60% of activity for tributyrin

transesterification after three cycles. ICP-OES revealed a negligible decrease in Ni:Al (Table S2) after the third recycle, suggesting that loss of activity was attributed to deactivation by poisoning of base sites or pore blockage by reaction intermediates [45].

There are few previous studies of NiAl LDH or NiO-derived catalysts for TAG transesterification, which hinders performance benchmarking, and of these all employed alkali precipitation syntheses and, hence, homogenous contributions to catalytic activity cannot be discounted [57,58]. Calcined NiAl and ZnAl LDHs are reported as inactive for sunflower oil transesterification with methanol at 65 °C [50]. Our reconstructed Ni_{4.1}Al LDH, which affords 14% trilaurin conversion (albeit at a higher temperature), is promising, despite their essentially microporous nature arising from a lamellar structure [59] with layer spacing of 0.3 nm observed in HRTEM (Figure S4), which hinders access of bulky TAGs to interlayers and in-pore base sites. Hence, most TAG activation is expected to occur over the external surface of the 2D NiAl LDH lamellar sheets in the sand rose structure observed in Figure 2c. The introduction of meso- and macroporosity is expected to significantly enhance TAG accessibility; hence, alkali-free, hydrothermally activated NiAl LDHs show potential as heterogeneous solid base catalysts for transesterification.

3. Experimental

3.1. Catalyst Synthesis

All reagents were of analytical grade and were used without further purification. Ni_xAl LDHs were synthesized in a 500 mL Radley's reactor-ready stirred vessel. Aqueous solutions of Ni(NO₃)₂·6H₂O (1.5 M) and Al(NO₃)₃·9H₂O (1.5 M) were mixed together in desired proportions to yield Ni:Al molar ratios spanning 1.5 to 4, with a final solution volume of 100 cm³. Ammonium carbonate (2 M, 100 cm³) was used as the precipitating agent and was added by a syringe pump (1 mL·min⁻¹) to the metal nitrate mixture while being stirred. Once the addition of metal nitrate and ammonium carbonate solutions was completed, ammonia solution was added dropwise to maintain a constant pH of 9.5. The mixture was aged while stirring at 65 °C for 18 h, after which the resulting precipitate was filtered and washed repeatedly with deionised water until the washings were pH 7. The resulting solid powder was then calcined at 350 °C (ramp rate of 1 °C·min⁻¹) for 5 h under flowing O₂ (20 mL·min⁻¹). The calcined solid was subjected to hydrothermal treatment in 50 mL of water, in a stirred Teflon-lined autoclave at 110 °C under autogenous pressure for 12 h. The treated solid was recovered by centrifugation and oven-dried at 80 °C before being stored in a vacuum desiccator prior to use.

3.2. Catalyst Characterisation

Powder X-ray diffraction was performed on a Bruker D8 ADVANCE diffractometer (Coventry, UK) using Cu K_α X-ray radiation (0.15418 nm). The diffraction patterns were recorded between 2θ = 10–80°. Crystallite sizes were determined by application of the Scherrer equation. The ratio of LDH:NiO following reconstruction was determined from the relative heights of the most intense reflections for NiAl LDH (13.8°) and NiO (43.6°). X-ray photoelectron spectroscopy was performed on a Kratos Axis HSi spectrometer (Manchester, UK) fitted with a charge neutralizer and magnetic focusing lens employing monochromated Al K_α radiation at 90 W. Spectral fitting was performed using CasaXPS version 2.3.16, with binding energies referenced to the C 1s Peak at 284.5 eV. N₂ porosimetry was undertaken on a Quantachrome Nova 4000 porosimeter (Hook, UK) on samples degassed at 120 °C for 3 h. Surface areas were calculated by the Brunauer–Emmett–Teller (BET) method from the desorption isotherm for P/P₀ < 0.2. Base site densities were determined by CO₂ pulse titration using a Quantachrome ChemBET 3000 chemisorption analyzer (Hook, UK) with a thermal conductivity detector. Then, 50 mg of the sample was placed in a quartz cell, outgassed for 1 h under flowing He at 120 °C, cooled to 40 °C, and then titrated with 50 μL CO₂ pulses at room temperature until uptake saturated. Thermogravimetric analysis with online mass spectrometry (TGA-MS) was performed on a Mettler Toledo TGA/DSC2 Star system (Leicester, UK) under flowing nitrogen during sample heating to

800 °C at 10 °C·min⁻¹. TGA was performed under N₂ to avoid any complications from oxidation of defects formed when a loss of H₂O/CO₂ would complicate the calculation of absolute mass loss during the TGA experiment. Scanning electron microscopy (SEM) was performed on a JEOL JSM-7000F microscope fitted with an energy dispersive X-ray spectroscopy detector (EDS) (Welwyn Garden City, UK) using an accelerating voltage of 20 kV. Transmission electron microscopy (TEM) analysis was carried out using a JEOL 2100F FEG STEM microscope operating at 200 keV. Samples were dispersed in methanol and drop cast onto copper grids coated with a holey carbon film (Agar Scientific Ltd., Essex, UK).

3.3. Catalytic Activity

Transesterification was performed using Radley's Starfish reactor, equipped with ACETM pressure flasks (Vineland, NJ, USA) modified with a dip tube to enable aliquots to be periodically withdrawn. Reactions were performed at 110 °C, using 10 mmol of triglyceride (TAG) and 308 mmol (12.5 mL) methanol, with 0.0025 mol (0.59 cm³) dihexyl ether as the internal standard; an additional 20 wt% 1-butanol was introduced for longer chain C₈-C₁₂ TAGs (tricaprylin and trilaurin, 99%, Alfa Aesar (Lancashire, UK) to improve their miscibility. Aliquots were periodically withdrawn during reaction. They were then filtered and diluted with dichloromethane, and analyzed by off-line gas chromatography (GC) using a Varian 450-GC (Crawley, UK) fitted with a Phenomenex (California, USA) ZB-5HT Inferno capillary column (15 m × 0.32 mm × 0.1 µm) for C₄-C₈ TAGs. Heavier TAGs were analyzed using a temperature-programmed, on-column injector and a Phenomenex ZB-1HT Inferno wide-bore capillary column (15 m × 0.53 mm × 0.1 µm). Turnover frequencies (TOFs) were calculated by normalizing initial rates of TAG conversion derived from the linear portion of reaction profiles (<20% conversion) to base site loadings obtained from CO₂ chemisorption. Triglyceride conversion and selectivity to fatty acid methyl ester (FAME) were calculated as follows:

$$\text{Conversion} = \frac{\text{Concentration of TAG at } T = 0 \text{ (mol/L)} - \text{Concentration of TAG at } T = t \text{ (mol/L)}}{\text{Concentration of TAG at } T = 0 \text{ (mol/L)}} \times 100 \quad (1)$$

$$\text{Selectivity} = \frac{\text{Concentration of product formed (mol/L)}}{\text{Total product concentration (mol/L)}} \times 100 \quad (2)$$

Leaching studies were conducted by hot filtration and recycle tests to establish the catalyst stability during tributyrin transesterification in methanol at 110 °C. The recovered catalyst was filtered between recycles, repeatedly washed with methanol to remove weakly bound residues, and then dried at 80 °C. After the third cycle, the catalyst was analyzed by ICP-OES to determine the final Ni and Al content.

4. Conclusions

NiAl LDHs with Ni:Al molar ratios spanning 1.5–4.1 were synthesized via an alkali-free route using NH₄OH and NH₄CO₃ as pH regulator and precipitant, respectively. The influence of activation protocol on 350 °C calcined Ni_xAl LDH was explored, with hydrothermal reconstruction at 110 °C proving to be the most effective for regenerating the parent LDH crystalline lamellar structure and maximizing base site loading. The extent of hydrothermal regeneration increased with Ni:Al ratio, attributed to suppressed NiO and AlO_x phase separation during calcination for higher Ni content. Base site loading increased with Ni content, attributed to undercoordinated oxygen sites as Al³⁺ is replaced by Ni²⁺, and/or increased surface hydroxyls on lamellae. The initial rates of tributyrin transesterification with methanol (and final conversion) increased with Ni loading and, hence, the base site density. However, TOFs also increased with Ni:Al ratio, indicative of a change in base site strength or accessibility across the family (the latter consistent with enhanced reconstruction). The most active Ni_{4.1}Al LDH catalyst was moderately stable towards site-blocking, and effective for the transesterification of C₄-C₁₂ triglycerides to FAMEs. Future work will explore the versatility of these catalysts for transesterification of

real oil feedstocks and the development of macroporous architectures in order to improve the mass transport of bulky TAGs. The somewhat weaker basicity of NiAl versus MgAl LDH counterparts may be advantageous with respect to poisoning by fatty acid impurities or adventitious CO₂.

Supplementary Materials: The following are available online: <https://www.mdpi.com/article/10.3390/catal12030286/s1>, Bulk and surface Ni content by XPS and EDS; XPS, TGA, XRD, HRTEM, and transesterification reaction profiles, conversion and selectivity following catalyst recycle tests, and elemental analysis of recycled catalyst. Figure S1. (a) Ni surface and bulk loading of NiAl LDHs determined by XPS and EDS respectively; (b) High-resolution XP spectra of NiAl LDHs with nominal Ni:Al atomic ratios of (i) 1.5, (ii) 3 and (iii) 4; Figure S2. Thermogravimetric analysis of NiAl LDHs with nominal Ni:Al atomic ratios of (A) 1.5, (B) 3 and (C) 4; Figure S3. Powder XRD patterns of Ni₄Al LDH after different hydrothermal treatments; Figure S4. HRTEM images of (top) precipitated and (bottom) hydrothermally reconstructed Ni_{4.1}Al LDH. Hydrothermal treatment involved 350 °C calcination and subsequent 110 °C water treatment; Figure S5. Reaction profiles for C₄ TAG transesterification with methanol by NiAl LDH as a function of Ni:Al atomic ratio. Reaction conditions: 100 mg catalyst, 10 mmol of triglyceride (TAG), 308 mmol (12.5 mL) methanol with 0.0025 mol (0.59 cm³) dihexylether as internal standard. Reaction was done at 650 rpm, 110 °C for 24 h; Figure S6. Reaction profiles for C₄–C₁₂ TAG transesterification with methanol by reconstructed Ni_{4.1}Al LDH. Reaction conditions: 100 mg catalyst, 10 mmol of triglyceride (TAG), 308 mmol (12.5 mL) methanol with 0.0025 mol (0.59 cm³) dihexylether as internal standard. 20 wt% 1-butanol was introduced for longer chain C₈–C₁₂ TAGs (tricaprylin and trilaurin) to improve their miscibility. Reaction was performed at 110 °C, 650 rpm, for 24 hours; Figure S7. Recycling of hydrothermally reconstructed Ni₄Al LDH in the transesterification of tributyrin with methanol. Reactions conditions: 100 mg catalyst, 110 °C, 10 mmol tributyrin (TAG), 30:1 methanol:TAG molar ratio, 650 rpm stirring, 24 h reaction; Table S1. Weight losses from TGA; Table S2. ICP-OES analysis on reconstructed Ni₄Al LDH after 3 recycles.

Author Contributions: Conceptualization, K.W. and A.F.L.; Data curation, N.A.T.; Formal analysis, N.A.T.; Investigation, N.A.T.; Methodology, J.C.M.; Supervision, J.C.M., A.F.L. and K.W.; Writing—original draft, N.A.T.; Writing—review and editing, A.F.L. and K.W. All authors have read and agreed to the published version of the manuscript.

Funding: This research was funded through a grant to N.A.T. from the University of Technology MARA (UiTM) under the Young Talent Research Grant (600-RMC/YTR/5/3 (017/2020)). K.W. and A.F.L. acknowledge the Australian Research Council for funding under DP200100204 and DP200100313.

Data Availability Statement: Data is available from the corresponding author on request.

Acknowledgments: We also acknowledge Lee Durndell (University of Plymouth) and Christopher Parlett (University of Manchester and Diamond Light Source) for assistance with HRTEM and Mark Issacs (University College London and HarwellXPS—EPSRC National Facility for XPS) for XPS measurements.

Conflicts of Interest: The authors declare no conflict of interest.

References

1. Yan, K.; Liu, Y.; Lu, Y.; Chai, J.; Sun, L. Catalytic application of layered double hydroxide-derived catalysts for the conversion of biomass-derived molecules. *Catal. Sci. Technol.* **2017**, *7*, 1622–1645. [[CrossRef](#)]
2. Song, Y.; Beaumont, S.K.; Zhang, X.; Wilson, K.; Lee, A.F. Catalytic applications of layered double hydroxides in biomass valorisation. *Curr. Opin. Green Sustain. Chem.* **2020**, *22*, 29–38. [[CrossRef](#)]
3. Jing, C.; Zhang, Q.; Liu, X.; Chen, Y.; Wang, X.; Xia, L.; Zeng, H.; Wang, D.; Zhang, W.; Dong, F. Design and fabrication of hydrotalcite-like ternary NiMgAl layered double hydroxide nanosheets as battery-type electrodes for high-performance supercapacitors. *RSC Adv.* **2019**, *9*, 9604–9612. [[CrossRef](#)]
4. Li, R.; Hu, Z.; Shao, X.; Cheng, P.; Li, S.; Yu, W.; Lin, W.; Yuan, D. Large Scale Synthesis of NiCo Layered Double Hydroxides for Superior Asymmetric Electrochemical Capacitor. *Sci. Rep.* **2016**, *6*, 18737. [[CrossRef](#)] [[PubMed](#)]
5. Szilagy, I. Layered Double Hydroxide-Based Nanomaterials—From Fundamentals to Applications. *Nanomaterials* **2019**, *9*, 1174. [[CrossRef](#)]

6. Tokudome, Y.; Tarutani, N.; Nakanishi, K.; Takahashi, M. Layered double hydroxide (LDH)-based monolith with interconnected hierarchical channels: Enhanced sorption affinity for anionic species. *J. Mater. Chem. A* **2013**, *1*, 7702–7708. [[CrossRef](#)]
7. Wang, Y.; Yan, D.; El Hankari, S.; Zou, Y.; Wang, S. Recent Progress on Layered Double Hydroxides and Their Derivatives for Electrocatalytic Water Splitting. *Adv. Sci.* **2018**, *5*, 1800064. [[CrossRef](#)]
8. Cavani, F.; Trifirò, F.; Vaccari, A. Hydrotalcite-type anionic clays: Preparation, properties and applications. *Catal. Today* **1991**, *11*, 173–301. [[CrossRef](#)]
9. Wang, Q.; O'Hare, D. Recent Advances in the Synthesis and Application of Layered Double Hydroxide (LDH) Nanosheets. *Chem. Rev.* **2012**, *112*, 4124–4155. [[CrossRef](#)]
10. Taviot-Guého, C.; Prévot, V.; Forano, C.; Renaudin, G.; Mousty, C.; Leroux, F. Tailoring Hybrid Layered Double Hydroxides for the Development of Innovative Applications. *Adv. Funct. Mater.* **2018**, *28*, 1703868. [[CrossRef](#)]
11. Tonelli, D.; Gualandi, I.; Musella, E.; Scavetta, E. Synthesis and Characterization of Layered Double Hydroxides as Materials for Electrocatalytic Applications. *Nanomaterials* **2021**, *11*, 725. [[CrossRef](#)] [[PubMed](#)]
12. Valente, J.S.; Lima, E.; Toledo-Antonio, J.A.; Cortes-Jacome, M.A.; Lartundo-Rojas, L.; Montiel, R.; Prince, J. Comprehending the Thermal Decomposition and Reconstruction Process of Sol–Gel MgAl Layered Double Hydroxides. *J. Phys. Chem. C* **2010**, *114*, 2089–2099. [[CrossRef](#)]
13. Mascolo, G.; Mascolo, M.C. On the synthesis of layered double hydroxides (LDHs) by reconstruction method based on the “memory effect”. *Microporous Mesoporous Mater.* **2015**, *214*, 246–248. [[CrossRef](#)]
14. Cao, Z.; Li, B.; Sun, L.; Li, L.; Xu, Z.P.; Gu, Z. 2D Layered Double Hydroxide Nanoparticles: Recent Progress toward Preclinical/Clinical Nanomedicine. *Small Methods* **2020**, *4*, 1900343. [[CrossRef](#)]
15. Dewangan, N.; Hui, W.M.; Jayaprakash, S.; Bawah, A.-R.; Poerjoto, A.J.; Jie, T.; Jangam, A.; Hidajat, K.; Kawi, S. Recent progress on layered double hydroxide (LDH) derived metal-based catalysts for CO₂ conversion to valuable chemicals. *Catal. Today* **2020**, *356*, 490–513. [[CrossRef](#)]
16. Takehira, K. Recent development of layered double hydroxide-derived catalysts—Rehydration, reconstitution, and supporting, aiming at commercial application. *Appl. Clay Sci.* **2017**, *136*, 112–141. [[CrossRef](#)]
17. Tang, S.; Yao, Y.; Chen, T.; Kong, D.; Shen, W.; Lee, H.K. Recent advances in the application of layered double hydroxides in analytical chemistry: A review. *Anal. Chim. Acta* **2020**, *1103*, 32–48. [[CrossRef](#)]
18. Yang, Z.-Z.; Zhang, C.; Zeng, G.-M.; Tan, X.-F.; Wang, H.; Huang, D.-L.; Yang, K.-H.; Wei, J.-J.; Ma, C.; Nie, K. Design and engineering of layered double hydroxide based catalysts for water depollution by advanced oxidation processes: A review. *J. Mater. Chem. A* **2020**, *8*, 4141–4173. [[CrossRef](#)]
19. Birjega, R.; Vlad, A.; Matei, A.; Ion, V.; Luculescu, C.; Dinescu, M.; Zavoianu, R. Growth and characterization of ternary Ni, Mg–Al and Ni–Al layered double hydroxides thin films deposited by pulsed laser deposition. *Thin Solid Film.* **2016**, *614*, 36–41. [[CrossRef](#)]
20. Stevens, M.B.; Enman, L.J.; Korkus, E.H.; Zaffran, J.; Trang, C.D.; Asbury, J.; Kast, M.G.; Toroker, M.C.; Boettcher, S.W. Ternary Ni-Co-Fe oxyhydroxide oxygen evolution catalysts: Intrinsic activity trends, electrical conductivity, and electronic band structure. *Nano Res.* **2019**, *12*, 2288–2295. [[CrossRef](#)]
21. Clause, O.; Rebours, B.; Merlen, E.; Trifirò, F.; Vaccari, A. Preparation and characterization of nickel-aluminum mixed oxides obtained by thermal decomposition of hydrotalcite-type precursors. *J. Catal.* **1992**, *133*, 231–246. [[CrossRef](#)]
22. Yue, X.; Zhang, L.; Sun, L.; Gao, S.; Gao, W.; Cheng, X.; Shang, N.; Gao, Y.; Wang, C. Highly efficient hydrodeoxygenation of lignin-derivatives over Ni-based catalyst. *Appl. Catal. B Environ.* **2021**, *293*, 120243. [[CrossRef](#)]
23. Li, D.; Lu, M.; Aragaki, K.; Koike, M.; Nakagawa, Y.; Tomishige, K. Characterization and catalytic performance of hydrotalcite-derived Ni-Cu alloy nanoparticles catalysts for steam reforming of 1-methylnaphthalene. *Appl. Catal. B Environ.* **2016**, *192*, 171–181. [[CrossRef](#)]
24. Sturgeon, M.R.; O'Brien, M.H.; Ciesielski, P.N.; Katahira, R.; Kruger, J.S.; Chmely, S.C.; Hamlin, J.; Lawrence, K.; Hunsinger, G.B.; Foust, T.D.; et al. Lignin depolymerisation by nickel supported layered-double hydroxide catalysts. *Green Chem.* **2014**, *16*, 824–835. [[CrossRef](#)]
25. Theiss, F.L.; Ayoko, G.A.; Frost, R.L. Synthesis of layered double hydroxides containing Mg²⁺, Zn²⁺, Ca²⁺ and Al³⁺ layer cations by co-precipitation methods—A review. *Appl. Surf. Sci.* **2016**, *383*, 200–213. [[CrossRef](#)]
26. Olf, H.W.; Torres-Dorante, L.O.; Eckelt, R.; Kosslick, H. Comparison of different synthesis routes for Mg–Al layered double hydroxides (LDH): Characterization of the structural phases and anion exchange properties. *Appl. Clay Sci.* **2009**, *43*, 459–464. [[CrossRef](#)]
27. Cantrell, D.G.; Gillie, L.J.; Lee, A.F.; Wilson, K. Structure-reactivity correlations in MgAl hydrotalcite catalysts for biodiesel synthesis. *Appl. Catal. A: Gen.* **2005**, *287*, 183–190. [[CrossRef](#)]
28. Tajuddin, N.A.; Manayil, J.C.; Isaacs, M.A.; Parlett, C.M.A.; Lee, A.F.; Wilson, K. Alkali-Free Zn–Al Layered Double Hydroxide Catalysts for Triglyceride Transesterification. *Catalysts* **2018**, *8*, 667. [[CrossRef](#)]
29. Jiang, L.; Guo, H.; Li, C.; Zhou, P.; Zhang, Z. Selective cleavage of lignin and lignin model compounds without external hydrogen, catalyzed by heterogeneous nickel catalysts. *Chem. Sci.* **2019**, *10*, 4458–4468. [[CrossRef](#)] [[PubMed](#)]
30. Ye, H.; Liu, S.; Yu, D.; Zhou, X.; Qin, L.; Lai, C.; Qin, F.; Zhang, M.; Chen, W.; Chen, W.; et al. Regeneration mechanism, modification strategy, and environment application of layered double hydroxides: Insights based on memory effect. *Coord. Chem. Rev.* **2022**, *450*, 214253. [[CrossRef](#)]

31. Yuan, Z.; Bak, S.-M.; Li, P.; Jia, Y.; Zheng, L.; Zhou, Y.; Bai, L.; Hu, E.; Yang, X.-Q.; Cai, Z.; et al. Activating Layered Double Hydroxide with Multivacancies by Memory Effect for Energy-Efficient Hydrogen Production at Neutral pH. *ACS Energy Lett.* **2019**, *4*, 1412–1418. [CrossRef]
32. Kikhtyanin, O.; Lesnik, E.; Kubička, D. The occurrence of Cannizzaro reaction over Mg-Al hydrotalcites. *Appl. Catal. A Gen.* **2016**, *525*, 215–225. [CrossRef]
33. Rocha, J.; del Arco, M.; Rives, V.; Ulibarri, A.M. Reconstruction of layered double hydroxides from calcined precursors: A powder XRD and ²⁷Al MAS NMR study. *J. Mater. Chem.* **1999**, *9*, 2499–2503. [CrossRef]
34. Pérez-Ramírez, J.; Mul, G.; Kapteijn, F.; Moulijn, J.A. On the stability of the thermally decomposed Co-Al hydrotalcite against retrotopotactic transformation. *Mater. Res. Bull.* **2001**, *36*, 1767–1775. [CrossRef]
35. Sato, T.; Fujita, H.; Endo, T.; Shimada, M.; Tsunashima, A. Synthesis of hydrotalcite-like compounds and their physico-chemical properties. *React. Solids* **1988**, *5*, 219–228. [CrossRef]
36. Prinetto, F.; Ghiotti, G.; Graffin, P.; Tichit, D. Synthesis and characterization of sol-gel Mg/Al and Ni/Al layered double hydroxides and comparison with co-precipitated samples. *Microporous Mesoporous Mater.* **2000**, *39*, 229–247. [CrossRef]
37. Belskaya, O.; Leont'eva, N.; Gulyaeva, T.; Cherepanova, S.; Talzi, V.; Drozdov, V.; Likholobov, V. Influence of a doubly charged cation nature on the formation and properties of mixed oxides MAIO_x (M= Mg²⁺, Zn²⁺, Ni²⁺) obtained from the layered hydroxide precursors. *Russ. Chem. Bull.* **2013**, *62*, 2349–2361. [CrossRef]
38. Cherepanova, S.V.; Leont'eva, N.N.; Arbuzov, A.B.; Drozdov, V.A.; Belskaya, O.B.; Antonicheva, N.V. Structure of oxides prepared by decomposition of layered double Mg–Al and Ni–Al hydroxides. *J. Solid State Chem.* **2015**, *225*, 417–426. [CrossRef]
39. Claydon, R.; Wood, J. A Mechanistic Study of Layered-Double Hydroxide (LDH)-Derived Nickel-Enriched Mixed Oxide (Ni-MMO) in Ultradispersed Catalytic Pyrolysis of Heavy Oil and Related Petroleum Coke Formation. *Energy Fuels* **2019**, *33*, 10820–10832. [CrossRef]
40. Naumkin, A.V.; Gaarenstroom, S.W.; Cedric, J. NIST Standard Reference Database 20, Version 4.1. Available online: <https://srdata.nist.gov/xps> (accessed on 22 November 2021).
41. Abelló, S.; Bolshak, E.; Gispert-Guirado, F.; Farriol, X.; Montané, D. Ternary Ni–Al–Fe catalysts for ethanol steam reforming. *Catal. Sci. Technol.* **2014**, *4*, 1111–1122. [CrossRef]
42. Li, C.; Wang, L.; Wei, M.; Evans, D.G.; Duan, X. Large oriented mesoporous self-supporting Ni–Al oxide films derived from layered double hydroxide precursors. *J. Mater. Chem.* **2008**, *18*, 2666–2672. [CrossRef]
43. Kovanda, F.; Rojka, T.; Bezdička, P.; Jiráťová, K.; Obalová, L.; Pacultová, K.; Bastl, Z.; Grygar, T. Effect of hydrothermal treatment on properties of Ni–Al layered double hydroxides and related mixed oxides. *J. Solid State Chem.* **2009**, *182*, 27–36. [CrossRef]
44. Trifirò, F.; Vaccari, A.; Clause, O. Nature and properties of nickel-containing mixed oxides obtained from hydrotalcite-type anionic clays. *Catal. Today* **1994**, *21*, 185–195. [CrossRef]
45. Woodford, J.J.; Dacquín, J.-P.; Wilson, K.; Lee, A.F. Better by design: Nanoengineered macroporous hydrotalcites for enhanced catalytic biodiesel production. *Energy Environ. Sci.* **2012**, *5*, 6145–6150. [CrossRef]
46. Prestopino, G.; Arrabito, G.; Generosi, A.; Mattoccia, A.; Paci, B.; Perez, G.; Verona-Rinati, G.; Medaglia, P.G. Emerging switchable ultraviolet photoluminescence in dehydrated Zn/Al layered double hydroxide nanoplatelets. *Sci. Rep.* **2019**, *9*, 11498. [CrossRef]
47. Nishimura, S.; Takagaki, A.; Ebitani, K. Characterization, synthesis and catalysis of hydrotalcite-related materials for highly efficient materials transformations. *Green Chem.* **2013**, *15*, 2026–2042. [CrossRef]
48. Gonçalves, A.A.S.; Costa, M.J.F.; Zhang, L.; Ciesielczyk, F.; Jaroniec, M. One-Pot Synthesis of MeAl₂O₄ (Me = Ni, Co, or Cu) Supported on γ -Al₂O₃ with Ultralarge Mesopores: Enhancing Interfacial Defects in γ -Al₂O₃ to Facilitate the Formation of Spinel Structures at Lower Temperatures. *Chem. Mater.* **2018**, *30*, 436–446. [CrossRef]
49. Creasey, J.J.; Chieragato, A.; Manayil, J.C.; Parlett, C.M.A.; Wilson, K.; Lee, A.F. Alkali- and nitrate-free synthesis of highly active Mg–Al hydrotalcite-coated alumina for FAME production. *Catal. Sci. Technol.* **2014**, *4*, 861–870. [CrossRef]
50. Sankaranarayanan, S.; Antonyraj, C.A.; Kannan, S. Transesterification of edible, non-edible and used cooking oils for biodiesel production using calcined layered double hydroxides as reusable base catalysts. *Bioresour. Technol.* **2012**, *109*, 57–62. [CrossRef]
51. Montero, J.M.; Brown, D.R.; Gai, P.L.; Lee, A.F.; Wilson, K. In situ studies of structure–reactivity relations in biodiesel synthesis over nanocrystalline MgO. *Chem. Eng. J.* **2010**, *161*, 332–339. [CrossRef]
52. Rabee, A.; Manayil, J.; Isaacs, M.; Parlett, C.; Durndell, L.; Zaki, M.; Lee, A.; Wilson, K. On the Impact of the Preparation Method on the Surface Basicity of Mg–Zr Mixed Oxide Catalysts for Tributyrin Transesterification. *Catalysts* **2018**, *8*, 228. [CrossRef]
53. Asakuma, Y.; Maeda, K.; Kuramochi, H.; Fukui, K. Theoretical study of the transesterification of triglycerides to biodiesel fuel. *Fuel* **2009**, *88*, 786–791. [CrossRef]
54. Kaneda, K.; Mizugaki, T. Design of high-performance heterogeneous catalysts using hydrotalcite for selective organic transformations. *Green Chem.* **2019**, *21*, 1361–1389. [CrossRef]
55. Chantrasa, A.; Phlernjai, N.; Goodwin, J.G. Kinetics of hydrotalcite catalyzed transesterification of tricaprilyn and methanol for biodiesel synthesis. *Chem. Eng. J.* **2011**, *168*, 333–340. [CrossRef]
56. Woodford, J.J.; Parlett, C.M.A.; Dacquín, J.-P.; Cibir, G.; Dent, A.; Montero, J.; Wilson, K.; Lee, A.F. Identifying the active phase in Cs-promoted MgO nanocatalysts for triglyceride transesterification. *J. Chem. Technol. Biotechnol.* **2014**, *89*, 73–80. [CrossRef]
57. Bin Jumrah, M.N.; Ibrahim, S.M.; Al-Huqail, A.A.; Bin-Murddhi, N.S.; Allam, A.A.; Abu-Taweel, G.M.; Altoom, N.; Al-Anazi, K.M.; Abukhadra, M.R. Enhancing the Catalytic Performance of NiO during the Transesterification of Waste Cooking Oil Using a Diatomite Carrier and an Integrated NiO Metal: Response Surface Studies. *ACS Omega* **2021**, *6*, 12318–12330. [CrossRef]

-
58. Cross, H.E.; Brown, D.R. Entrained sodium in mixed metal oxide catalysts derived from layered double hydroxides. *Catal. Commun.* **2010**, *12*, 243–245. [[CrossRef](#)]
 59. Gonzalez Rodriguez, P.; de Ruiter, M.; Wijnands, T.; ten Elshof, J.E. Porous Layered Double Hydroxides Synthesized using Oxygen Generated by Decomposition of Hydrogen Peroxide. *Sci. Rep.* **2017**, *7*, 481. [[CrossRef](#)] [[PubMed](#)]